Mechanical Systems and Signal Processing 163 (2022) 108186

Contents lists available at ScienceDirect

Mechanical Systems and Signal Processing

journal homepage: www.elsevier.com/locate/ymssp

Deterministic and statistical methods for the characterisation of poroelastic media from multi-observation sound absorption measurements

J. Cuenca [a], P. Göransson [b,*], L. De Ryck [a], T. Lähivaara [c]

[a] Siemens Industry Software, Interleuvenlaan 68, BE-3001 Leuven, Belgium
[b] Department of Aeronautical and Vehicle Engineering, KTH Royal Institute of Technology, Teknikringen 8, SE-10044 Stockholm, Sweden
[c] Department of Applied Physics, University of Eastern Finland, P.O. Box 1627, FIN-70211 Kuopio, Finland

ARTICLE INFO

Communicated by Annie Ross

Keywords:
Poroelastic media
Parameter estimation
Coupled problems
Deterministic framework
Bayesian framework
Uncertainty quantification

ABSTRACT

This paper proposes a framework for the estimation of the transport and elastic properties of open-cell poroelastic media based on sound absorption measurements. The sought properties are the Biot-Johnson-Champoux-Allard model parameters, namely five transport parameters, two elastic properties and the mass density, as well as the sample thickness. The methodology relies on a multi-observation approach, consisting in combining multiple independent measurements into a single dataset, with the aim of over-determining the problem. In the present work, a poroelastic sample is placed in an impedance tube and tested in two loading conditions, namely in a rigid-backing configuration and coupled to a resonant expansion chamber. Given the non-monotonic nature of the experimental data, an incremental parameter estimation procedure is used in order to guide the model parameters towards the global solution without terminating at local minima. A statistical inversion approach is also discussed, providing refined point estimates, uncertainty ranges and parameter correlations. The methodology is applied to the characterisation of a sample of melamine foam and provides estimates of all nine parameters with compact uncertainty ranges. It is shown that the model parameters are retrieved with a lower uncertainty in the multi-observation case, as compared with a single-observation case. The method proposed here does not require prior knowledge of the thickness or any of the properties of the sample, and can be carried out with a standard two-microphone impedance tube.

1. Introduction

The estimation of material and geometrical properties of mechanical and acoustical systems is central to many areas of engineering, yet numerous methodological challenges exist. One such example, of particular interest here, is the measurement of transport and elastic properties of poroelastic media. These materials exhibit intricate and complex fluid–structure interactions related to visco-thermal exchanges and visco-elastic energy dissipation, and as a result are often modelled with a large number of parameters. The estimation of a complete set of these parameters, which consistently and coherently satisfy a comprehensive constitutive model, has been a topic of increasing interest, for instance for its use in simulation tools, as computational power has grown over the last decades.

* Corresponding author.
E-mail addresses: jacques.cuenca@siemens.com (J. Cuenca), pege@kth.se (P. Göransson), laurent.deryck@siemens.com (L. De Ryck), timo.lahivaara@uef.fi (T. Lähivaara).

https://doi.org/10.1016/j.ymssp.2021.108186
Received 6 November 2020; Accepted 22 June 2021

1.1. Direct methods for individual parameters

A variety of methods for the characterisation of poroelastic media have been developed, including direct, indirect and inverse methods. Direct methods involve dedicated experimental rigs providing individual estimations of a subset of properties, e.g. porosity, tortuosity, thermal and flow permeability, viscous and thermal characteristic lengths, Young's modulus and mechanical loss factor [1–9]. These approaches are reliable and powerful in that a potentially high degree of accuracy is reached thanks to an appropriate control of experimental conditions and isolation of sources of error. Nevertheless, using individually measured parameters in a comprehensive simulation model may lead to inconsistencies. For instance, separate samples are often required for the different dedicated setups, thereby introducing variability due to inhomogeneity across samples. Also, the availability and maintenance of a full suite of test rigs is often impractical. As an alternative, indirect and inverse methods have been proposed, of which a selection is recalled below. An exhaustive review of all available methods is out of scope here and the reader is referred to the recent review by Horoshenkov [10] and references therein for a complementary overview.

1.2. Indirect methods

Indirect analytical methods rely on derivations of the constitutive properties from the intrinsic equivalent acoustical properties of the porous sample, namely its frequency-dependent equivalent density and bulk modulus, which can be measured using a three- or four-microphone transmission impedance tube, or a dual-load two-microphone tube. First proposed for the estimation of viscous and thermal dissipation properties by Panneton and Olny [11,12], the methodology has been reported by Bonfiglio and Pompoli [13] to provide all 5 parameters in the Johnson-Champoux-Allard (JCA) model [14,15] and recently by Jaouen et al. [16] for the measurement of all 6 parameters of the Johnson-Champoux-Allard-Lafarge (JCAL) model [14,15,17]. Such an indirect methodology is robust and mature, and allows for a comprehensive estimation of the full set of transport properties and their uncertainties. Nevertheless, these estimations are inherently dependent on a number of assumptions as well as on the accuracy of the measured intrinsic acoustical properties [11]. Additionally, a minor drawback is that the estimation of the porosity and flow resistivity rely on the manual identification of frequency ranges where the intrinsic acoustical quantities exhibit an asymptotic behaviour. Although this could be automated, practical considerations such as frequency resolution could influence the frequency ranges and potentially lead to an underestimation of parameter uncertainties. Complementary analytical approaches have been proposed, for instance by Groby et al. [18] for estimating transport properties from ultrasonic reflection and transmission measurements. The ultrasonic range inherently provides a direct comparison with the high-frequency approximation of the JCA model but does not provide access to the flow resistivity, thus requiring it to be measured separately.

1.3. Deterministic inverse methods

Inverse methods stand as an appealing alternative to direct and indirect methods in that the material properties are obtained as the set of model parameters yielding the best fit of a simulation based on the constitutive model. This guarantees that the solution is a feasible set of parameters that automatically satisfies the model, without the need for approximations or additional steps. A vast number of deterministic inverse methods have been developed and validated. For instance, methods have been proposed to estimate all, or a subset of, the transport parameters in the JCA or JCAL models using the measured complex characteristic impedance as the target data [13,19–21], which can be carried out in an impedance tube with transmission capabilities. Methods using a two-microphone tube have also been investigated. For instance, Dossi et al. [22] have proposed the additional estimation of the elastic parameters of polyurethane foams by combining datasets from specimens of different thicknesses. A method for estimating the 5 JCA parameters and 3 elastic properties has been proposed by Verdière et al. [23] relying on a numerical model accounting for intentional circumferential air gaps and using sound absorption measurements, assuming prior knowledge of the sample dimensions and density. A numerical model was also used by Vanhuyse et al. [24] to account for intentionally clamped circumferential boundaries. The retrieval of transport and elastic parameters from the reflection coefficient was numerically validated therein. In addition to impedance tube methods, deterministic inverse methods for the estimation of anisotropic transport and elastic properties [25–27] as well as methods relying on ultrasonic measurements [28,29] have been studied. In particular, Ogam et al. [30] proposed an ultrasonic time-domain method for the estimation of porosity, tortuosity, viscous characteristic length, density, Young's modulus and Poisson ratio.

1.4. Statistical inverse methods

Fully deterministic approaches lack however the ability to estimate uncertainty ranges for the model parameters. Chazot et al. [31] proposed a Bayesian framework for the estimation of 8 properties of poroelastic media, including mass density, 5 transport parameters and 2 elastic properties, including estimated confidence intervals for all the parameters. As such, the obtained solutions were not unique, and the mean estimates presented large deviations from reference values in general, the reported elasticity showing the largest estimation errors in particular. Nevertheless, the method demonstrates the feasibility of fully characterising poroelastic media using an impedance tube. Niskanen et al. [32] studied deterministic and statistical inverse methods for the estimation of the 6 parameters of the JCAL model. The method uses a transmission tube setup and provides point estimates, credible ranges and correlations between parameters using the equivalent density and bulk modulus as the target data. A two-microphone tube with a rigid-backed sample was investigated as an experimentally simpler alternative, where the difficulty of avoiding local minima was reported, as well as a higher

degree of inter-parameter correlation in the obtained solution. In further work, Niskanen et al. [33] discussed the estimation of transport and elastic properties of poroelastic media using reflection and transmission coefficients in the ultrasonic range. The work numerically demonstrates the feasibility of such an approach and allows for the estimation of shear properties by exciting the material in oblique incidence. Other notable studies include the works of Roncen et al. [34–36], who investigated the statistical inference of the transport properties of rigid porous media in the time domain, including a high order model of viscous effects. Fackler et al. [37] used a Bayesian framework for the characterisation of multi-layer rigid porous media in terms of the porosity, flow resistivity, tortuosity and thickness of the layers.

1.5. Motivation for the proposed method

The use of round robin tests has shown that acoustic measurements on porous media exhibit relatively poor inter-laboratory reproducibility [38,39]. The reported measurements included frequency-dependent characteristic impedance, complex wave-number and sound absorption coefficient. Nevertheless, up to 3 times better reproducibility was reported for sound absorption measurements in comparison to surface impedance [38], suggesting that the use of sound absorption in combination with an inverse method can potentially reduce uncertainties in the estimated parameters. A closed-form description of the behaviour of a rigidly backed isotropic poroelastic layer exists [40]. Assuming that this model applies as well to samples with longitudinally-sliding boundaries in a rigidly backed tube, it forms the basis for the model inversion in the present work. In this respect, the reduced amount of data inherent to a purely energetic quantity, as compared to complex quantities, could possibly add to the above-mentioned problems with parametric insensitivity and the associated convergence of the solution to a unique set of parameters. This is particularly true in the case of coupled resonant systems, whose inverse problems are subject to multiple local minima due to the non-monotonic nature of their frequency response.

Recent work by the authors proposes an incremental method for solving inverse problems in coupled resonant systems from the knowledge of their transfer function [41]. The method consists in solving the inverse problem in a series of steps, starting with a sub-problem in a frequency domain where the observed system exhibits an asymptotic behaviour, then gradually increasing the frequency span towards that of the full problem. Such an incremental method was shown to guide the design variables towards the global solution, while avoiding local minima. This approach has also been applied in preliminary numerical investigations aiming to estimate the properties of porous and poroelastic media [42,43], laying the ground for the present work.

1.6. Outline of the paper

This paper proposes an inverse method for the simultaneous estimation of a set of 9 properties of a poroelastic material sample using a two-microphone impedance tube. The target unknowns are the 5 transport parameters and 2 elastic properties within the Biot-Johnson-Champoux-Allard (Biot-JCA) model [14,15,40], the material density and the sample thickness. Here the previously mentioned incremental estimation method is augmented with a multi-observation approach, which is introduced with the aim of over-determining the problem. The multi-observation dataset consists of measurements of the sound absorption coefficient of a rigidly backed sample in two different loading conditions, namely with and without an expansion chamber. In order to ensure a gradual increase of the problem complexity, the sequence of sub-problems is defined by splitting the measured data into alternating monotonic segments [44]. In the present paper, the multiple sub-problems are solved in a deterministic sense using non-linear numerical optimisation. In order to assess the uncertainty of the parameter estimation, a statistical method within the Bayesian framework is then applied to the full problem as a means to obtain credible ranges and refined point estimates for the different model parameters.

The paper is organised as follows. Section 2 presents the proposed load cases, the model of the corresponding sound absorption coefficient and the experimental setup used. Section 3 formalises the multi-observation model and proposes a deterministic incremental inversion method as well as a statistical inversion method. The results of the approach are presented in Section 4 and a summary of the findings is given in Section 5.

2. Multi-observation problem

The aim of the work is to estimate the properties of a poroelastic material (PEM) sample from the knowledge of its sound absorption coefficient in one or various loading conditions. In the following paragraphs we propose a model of the sound absorption coefficient in the different loading conditions as well as an experimental implementation.

2.1. Model

The starting point is the model of the sound absorption coefficient in the different load cases as a function of the unknown material parameters of interest. As the objective is to estimate these parameters based on experimental data, the dimensions of the loading elements, which are subject to uncertainties, are considered unknown as well. Furthermore, visco-thermal losses at the tube walls are modelled using the approach in Ref. [45].

The two loading conditions considered in this work are depicted in Fig. 1. Case (A) consists of a rigidly-backed poroelastic sample at the end of a tube of length l_a. In case (B) the sample is loaded with three adjacent cylindrical duct elements of lengths l_b, l_e and l_c forming an expansion chamber of radius r_e, as illustrated in the figure. The tube of length l_c between the expansion chamber and the foam acts as a coupling element that can be tuned so as to maximise the influence of the elasticity of the foam on the overall sound

absorption.

The coupled system is modelled as a multi-layer system using the transfer matrix method [40]. The rigid-backed poroelastic material sample is modelled using the normal incidence impedance derived in [40,46], here denoted

$$Z_{\mathrm{PEM}}(\mathbf{x}_{\mathrm{PEM}}, \omega), \tag{1}$$

where ω is the circular frequency and

$$\mathbf{x}_{\mathrm{PEM}} = \{h, \rho, \phi, \sigma, \alpha_\infty, \Lambda, \Lambda', E, \eta\} \tag{2}$$

is the set of parameters governing the behaviour of the poroelastic sample, with h the thickness, ρ the mass density, ϕ the porosity, σ the static flow resistivity, α_∞ the high-frequency limit of the tortuosity, Λ the viscous characteristic length, Λ' the thermal characteristic length, E the Young's modulus and η the viscoelastic damping ratio. The estimation of these 9 parameters is the main objective of the paper. For the purposes of the present paper, the explicit expression of Eq. (1) will not be repeated here, for which the reader is referred to Refs. [40,46]. It is worth noting that due to the one-dimensional nature of the problem, the Young's modulus and the Poisson ratio cannot be measured as two independent variables. Therefore lateral deformation is here ignored by setting the Poisson ratio to zero.

For convenience in modelling the sudden area changes in load case (B), the transfer matrix method is here formulated in terms of the acoustic pressure and flow. The transfer matrices of the individual duct elements are given by [47]

$$\mathbf{T}_n = \begin{bmatrix} \cos(k_0 l_n) & \dfrac{iZ_0}{\pi r_n^2}\sin\left(k_0 l_n\right) \\ -\dfrac{\pi r_n^2}{iZ_0}\sin\left(k_0 l_n\right) & \cos(k_0 l_n) \end{bmatrix}, \quad n = \mathrm{a}, \mathrm{b}, \mathrm{e}, \mathrm{c}, \tag{3}$$

where $k_0 = \omega/c_0$ is the wavenumber in air and $Z_0 = \rho_0 c_0$ is the characteristic impedance of air, with c_0 the speed of sound and ρ_0 the mass density of air. The terms l_n and r_n denote the length and radius of the various duct elements, with $r_{\mathrm{a}} = r_{\mathrm{b}} = r_{\mathrm{c}}$. For load case (A), the transfer matrix of the tube between microphone 2 and the sample is denoted

$$\mathbf{T}^{(\mathrm{A})}\left(l_{\mathrm{a}}\right) = \mathbf{T}_{\mathrm{a}}. \tag{4}$$

For load case (B), the joint transfer matrix of the tube section, the expansion chamber and the cavity is

$$\mathbf{T}^{(\mathrm{B})}\left(\mathbf{x}_{\mathrm{load}}\right) = \mathbf{T}_{\mathrm{b}}\mathbf{T}_{\mathrm{e}}\mathbf{T}_{\mathrm{c}}, \tag{5}$$

where

$$\mathbf{x}_{\mathrm{load}} = \{l_{\mathrm{b}}, l_{\mathrm{e}}, r_{\mathrm{e}}, \eta_{\mathrm{b}}, \eta_{\mathrm{e}}, l_{\mathrm{c}}\} \tag{6}$$

are the parameters governing the behaviour of the expansion chamber and coupling tube. The complete set of variables of interest for load cases (A) and (B) can be denoted

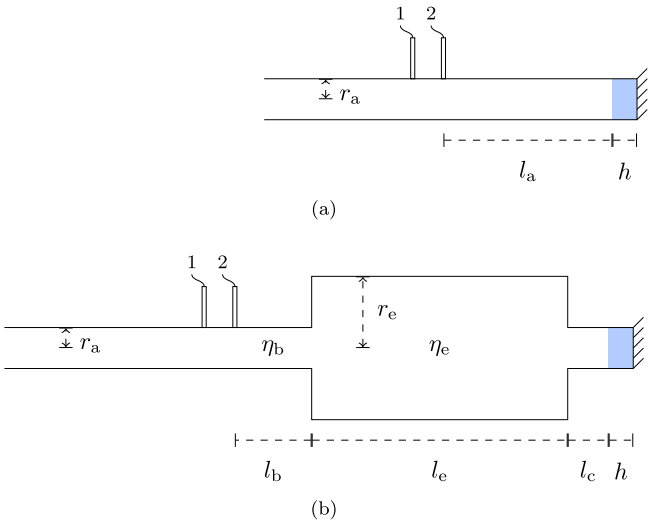

Fig. 1. Schematic representation of the impedance tube setup in the two loading conditions. (a) Load case (A): rigid-backed material sample; (b) load case (B): rigid-backed material sample coupled to expansion chamber.

$$\mathbf{x}^{(A)} = \mathbf{x}_{\mathrm{PEM}}, \tag{7}$$

$$\mathbf{x}^{(B)} = \{\mathbf{x}_{\mathrm{PEM}}, \mathbf{x}_{\mathrm{load}}\}, \tag{8}$$

which consist of 9 and 15 unknown parameters, respectively. The impedance of the coupled system is given by

$$Z_n\left(\mathbf{x}^{(n)}, \omega\right) = \frac{Z_{\mathrm{PEM}} T_{11}^{(n)} + T_{12}^{(n)} S}{Z_{\mathrm{PEM}} T_{21}^{(n)} / S + T_{22}^{(n)}}, \quad n = \mathrm{A}, \mathrm{B}, \tag{9}$$

where $S = \pi r_{\mathrm{a}}^2$ is the cross-section of the impedance tube and $T_{ij}^{(n)}$ are the components of the transfer matrix of load (A) or (B). The reflection coefficient of the compound system is then

$$R_n\left(\mathbf{x}^{(n)}, \omega\right) = \frac{Z_n(\mathbf{x}^{(n)}, \omega) - Z_0}{Z_n(\mathbf{x}^{(n)}, \omega) + Z_0}, \tag{10}$$

yielding the absorption coefficient as

$$\alpha_n\left(\mathbf{x}^{(n)}, \omega\right) = 1 - |R_n(\mathbf{x}^{(n)}, \omega)|^2. \tag{11}$$

2.2. Experimental setup

This section describes the experimental setup and provides the nominal values of the dimensions as depicted in Fig. 1, on which the model depends. Fig. 2 shows the impedance tube in load case (B) and the foam sample of interest.

The experimental setup relies on a Spectronics impedance tube with two G.R.A.S. 46BD 1/4" microphones with nominal sensitivity 1.45 mV/Pa, spaced by 29.21 mm, and the acquisition and processing are carried out via a Simcenter SCADAS Mobile 05 in Simcenter Testlab 17 "Sound absorption testing using impedance tube", following the procedure described in the international standard [1]. The calibration transfer functions and all subsequent acquisitions are performed under broadband random noise excitation using 100 non-overlapping Hann window averages. The frequency resolution of the measurements is 0.78125 Hz.

In order to achieve the loading condition illustrated in Fig. 1(a), the sample is placed in a secondary tube connected to the primary tube section. The loading condition illustrated in Fig. 1(b) is achieved by inserting an expansion chamber between the primary and secondary tube sections. The expansion chamber is made of aluminium, with acrylic lateral walls.

The sample of melamine foam was cut by hand to a thickness of $h = 24 \pm 1$ mm and attached to a rigid piston with double-sided tape. The piston comprises a seal around its circumference and is allowed to slide along the tube. The tube radius is provided by the manufacturer as $r_{\mathrm{a}} = 17.43$ mm and here assumed to be exact. The distance from microphone 2 to the modelled system was measured as $l_{\mathrm{a}} = 80 \pm 5$ mm in load case (A) and nominally as $\bar{l}_{\mathrm{b}} = 100 \pm 5$ mm in load case (B). The inner dimensions of the expansion chamber were measured as $r_{\mathrm{e}} = 63 \pm 2$ mm and $l_{\mathrm{e}} = 227 \pm 2$ mm.

The nominal length of the coupling tube between the expansion chamber and the foam is $\bar{l}_{\mathrm{c}} = 40 \pm 1$ mm. Because of the sudden area changes at the connection of this tube with the expansion chamber, a length correction [48–50] is required in order to account for inertial effects. The operational length of the coupling tube is thus estimated as $l_{\mathrm{c}} = 51.7 \pm 3.6$ mm, where the lower and upper limits are estimated in a conservative manner, corresponding to a tube of length $\bar{l}_{\mathrm{c}}$ connected to an expansion of radius r_{e} and to a baffled tube of length $\bar{l}_{\mathrm{c}} + h$, respectively. A similar reasoning for the length between microphone 2 and the expansion chamber yields $l_{\mathrm{b}} = 111.7 \pm 7.6$ mm.

Further required parameters are those related to the properties of air, whose values are here considered exact, namely the speed of sound $c_0 = 343$ m·s^{-1}, the mass density $\rho_0 = 1.204$ kg·m^{-3}, the atmospheric pressure $p_0 = 101320$ Pa, the dynamic viscosity $\mu_0 = 1.84{\cdot}10^{-5}$ kg·m^{-1}·s^{-1}, the ratio of specific heats $\gamma = 1.4$, and Prandtl's number $\mathrm{Pr} = 0.71$.

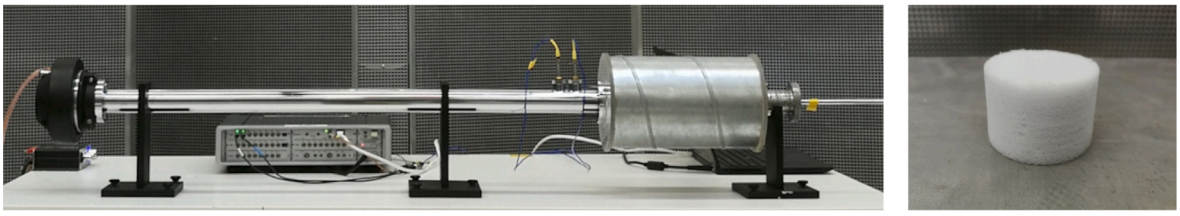

(a) (b)

Fig. 2. Experimental setup and material sample. (a) Impedance tube with expansion chamber and poroelastic material termination; (b) melamine foam sample.

3. Model inversion method

This section proposes an observation model and presents the different inversion methods here developed. In the present application, individual observations consist of a measurement of the frequency-dependent sound absorption coefficient in one of the two loading conditions (A) or (B), denoted α_n^{meas}, with $n = 1$ (load case (A)) or $n = 2$ (load case (B)). In this section, a generic notation g_n^{meas} with $n = 1, \ldots, N$ is preferred for the sake of generality.

3.1. Observation model

The experimental observation for a given load case n at circular frequency ω_m is denoted $g_n^{\text{meas}}(\omega_m)$ and assumed real-valued. It is further assumed that observations for different load cases are independent, that is, the outcome of any of the observations does not affect the others. It is then possible to construct a compound measurement $\mathbf{g}^{\text{meas}}$ by concatenating individual observations, as

$$\mathbf{g}^{\text{meas}} = \begin{bmatrix} [\, g_1^{\text{meas}}(\omega_1) & g_1^{\text{meas}}(\omega_2) & \cdots & g_1^{\text{meas}}(\omega_M)\,]^{\mathrm{T}} \\ [\, g_2^{\text{meas}}(\omega_1) & g_2^{\text{meas}}(\omega_2) & \cdots & g_2^{\text{meas}}(\omega_M)\,]^{\mathrm{T}} \\ & \vdots & & \\ [\, g_N^{\text{meas}}(\omega_1) & g_N^{\text{meas}}(\omega_2) & \cdots & g_N^{\text{meas}}(\omega_M)\,]^{\mathrm{T}} \end{bmatrix}, \tag{12}$$

where M is the number of frequency lines and N is the number of observations, yielding a dataset of size $(MN \times 1)$. It is assumed that the experimental observation differs from the model prediction by an error, such that

$$\mathbf{g}^{\text{meas}} = \mathbf{g}(\mathbf{x}_0) + \varepsilon, \tag{13}$$

where $\mathbf{g}(\mathbf{x}_0)$ is the mathematical model, evaluated at the true set of parameters $\mathbf{x}_0$, and ε is a random variable representing the modelling and measurement uncertainties. Here, we model ε as Gaussian, with zero mean and a diagonal covariance matrix $\Gamma_\varepsilon = \sigma_\varepsilon^2 \mathbf{I}$, where σ_ε^2 is the error variance and $\mathbf{I}$ denotes the identity matrix of size $(MN \times MN)$.

Owing to the existence of the error ε, the true set of model parameters $\mathbf{x}_0$ is inaccessible with complete certainty. The following paragraphs present different model inversion paradigms aiming at obtaining an estimate $\widetilde{\mathbf{x}}_0$ of the model parameters $\mathbf{x}_0$.

3.2. Deterministic inversion framework

A deterministic estimate of the model parameters can be obtained by minimising the difference between the experimental observation and the model prediction, as

$$\widetilde{\mathbf{x}}_0^{(\text{det})} = \underset{\mathbf{x}}{\operatorname{argmin}} f_{\text{obj}}\left(\mathbf{x}\right), \tag{14}$$

where

$$f_{\text{obj}}\left(\mathbf{x}\right) = \frac{1}{MN} \sum_{n=1}^{N} \sum_{m=1}^{M} \left(g_n^{\text{meas}}(\omega_m) - g_n(\mathbf{x}, \omega_m) \right)^2 \tag{15}$$

is the objective function, here defined as the residual sum of squares. The normalisation factor $1/MN$ is added in order to enable comparing residuals $f_{\text{obj}}(\widetilde{\mathbf{x}}_0^{(\text{det})})$ for observations comprising different numbers of frequency lines M or load cases N.

The minimisation of the objective function may be performed with any general purpose optimisation tool. Two solvers are used in the present work, namely a sequential quadratic programming algorithm (SQP) [51] and the globally convergent method of moving asymptotes (GCMMA) [52], as detailed later-on in Section 4. As a convergence and stopping criterion, tolerance factors $\delta_{f_{\text{obj}}}$ and $\delta_{\mathbf{x}}$ are set for the relative variation of the objective function and variables over a number n_{it} of consecutive iterations.

3.3. Incremental inversion

The above deterministic framework is here used within the incremental method developed by the authors in [41–43]. The model inversion procedure therein relies on a gradual complexification of the problem, starting from an asymptotic observation and terminating at the full desired problem. At each stage of the approach, the corresponding sub-problem is solved and the solution is used as the starting point for the next sub-problem. For frequency-dependent observations, the approach starts with a narrow low-frequency observation whose upper frequency limit is incrementally raised.

A common measure for the complexity of a real function is the number of alternating strictly monotonic segments [44]. In the present work, in order to ensure that the series of sub-problems yield a gradual increase of the complexity of the inverse problem, the frequency range is split into segments where the measured data is monotonic. The problem is solved from the lowest measured frequency to the upper limit of each monotonic segment sequentially, until reaching the full frequency range. In the case of a multi-

observation dataset, the upper limits of all monotonic segments across the different observations are used.

In the present work, the different steps in the incremental inversion are performed using the deterministic inversion framework detailed in Section 3.2. In addition, in order to capture the low-frequency asymptotic behaviour of the system, an initial frequency range is added as half the frequency span of the first monotonic section. Also, in order to ensure convergence of the estimated set of parameters, a final sub-problem is appended, where the tolerance factors are refined by a factor 10 and considered over a larger number of iterations.

3.4. Statistical inversion framework

In order to obtain a measure of the uncertainty on the model parameters of interest, the unknown quantities are modelled as random variables and the problem is formulated using a Bayesian framework [53,54]. The latter allows to evaluate the set of unknowns in a probabilistic sense, that is, by estimating their conditional probabilities for a given observation $\mathbf{g}^{\text{meas}}$. In this work, the unknown quantities of interest are the model parameters $\mathbf{x}$. In addition, the standard deviation of the error, σ_ε, is considered unknown, and modelled as a random variable as well. The conditional probability density of the set of unknowns for a given observation is given by Bayes' formula [53],

$$P(\mathbf{x},\sigma_\varepsilon|\mathbf{g}^{\text{meas}}) \sim P(\mathbf{g}^{\text{meas}}|\mathbf{x},\sigma_\varepsilon)P(\mathbf{x},\sigma_\varepsilon), \tag{16}$$

where $P(\mathbf{x},\sigma_\varepsilon|\mathbf{g}^{\text{meas}})$ is also referred to as the posterior density and $P(\mathbf{g}^{\text{meas}}|\mathbf{x},\sigma_\varepsilon)$ is the likelihood of the observation given the unknowns. The prior $P(\mathbf{x},\sigma_\varepsilon)$ is here assumed uniform across a sufficiently wide range within the admissible domain of the model parameters and of the standard deviation of the error. Owing to the assumption of a Gaussian error ε in the observation model (13), the likelihood can be expressed as

$$P\left(\mathbf{g}^{\text{meas}}\middle|\mathbf{x},\sigma_\varepsilon\right) = P_\varepsilon\left(\mathbf{g}^{\text{meas}} - \mathbf{g}\left(\mathbf{x}\right)\right) = \frac{1}{\sqrt{(2\pi)^{MN}\det(\Gamma_\varepsilon)}}\exp\left(-\frac{1}{2}(\mathbf{g}^{\text{meas}} - \mathbf{g}(\mathbf{x}))^{\mathrm{T}}\Gamma_\varepsilon^{-1}(\mathbf{g}^{\text{meas}} - \mathbf{g}(\mathbf{x}))\right), \tag{17}$$

where P_ε is the probability density of the error. Furthermore, the assumption that the covariance matrix of the error is diagonal yields

$$P\left(\mathbf{g}^{\text{meas}}\middle|\mathbf{x},\sigma_\varepsilon\right) = \frac{1}{\left(\sqrt{2\pi}\,\sigma_\varepsilon\right)^{MN}}\exp\left(-\frac{1}{2\sigma_\varepsilon^2}\sum_{n=1}^{N}\sum_{m=1}^{M}\left(g_n^{\text{meas}}(\omega_m) - g_n(\mathbf{x},\omega_m)\right)^2\right). \tag{18}$$

In the present work, the posterior density is sampled by means of a Markov Chain Monte Carlo method, using the Metropolis–Hastings algorithm with an adaptive proposal scheme [55,56]. The purpose of such a procedure is to visit the admissible domain of the unknowns with a probability $P(\mathbf{x},\sigma_\varepsilon|\mathbf{g}^{\text{meas}})$, where the jumps between successive points of the chain are determined by an adaptive proposal distribution. In practice, σ_ε is estimated together with the model parameters $\mathbf{x}$, such that the complete set of unknowns can be denoted

$$\mathbf{y} = \{\mathbf{x},\sigma_\varepsilon\}. \tag{19}$$

The proposal distribution is here defined as Gaussian, where its covariance matrix is initialised as diagonal and then adapted as a function of the covariance matrix of past samples [56], as

$$\mathbf{C}^{(j)} = \gamma_j\left(\operatorname{cov}\left(\mathbf{y}^{(0)},\ldots,\mathbf{y}^{(j-1)}\right) + \delta\mathbf{I}\right), \quad j \geqslant J, \tag{20}$$

where J is an arbitrary jump number at which the adaptation is started, δ is an arbitrarily small number and $\mathbf{I}$ denotes the identity matrix of size $(D\times D)$, D being the dimension of the problem, i.e. $D = 10$ for the single-observation case (load (A)) and $D = 16$ for the dual-observation case (loads (A) and (B)). The scaling parameter γ_j is initialised at [57]

$$\gamma_J = 2.38^2/D \tag{21}$$

and then updated following guidelines by Andrieu and Thoms [58] in order to reach the desired acceptance rate a_*. Here we choose

$$\gamma_{j+1} = \gamma_j\mu_{j+1}^{a_j - a_*}, \quad j \geqslant J, \tag{22}$$

where a_j is the acceptance rate at jump j and μ_j is an arbitrary strictly decreasing sequence converging to 1.

The solution provided by the deterministic inversion procedure, $\widetilde{\mathbf{x}}_0^{(\text{det})}$, is a feasible set of model parameters and therefore used as a starting point for the chain. This has the advantage of reducing the required number of iterations in the burn-in phase. Accordingly, an initial estimate of the standard deviation σ_ε of the error is obtained from Eq. (13) as

$$\widetilde{\sigma}_\varepsilon = \sqrt{\frac{1}{MN}\sum_{n=1}^{N}\sum_{m=1}^{M}\left(g_n^{\text{meas}}(\omega_m) - g_n\left(\widetilde{\mathbf{x}}_0^{(\text{det})},\omega_m\right)\right)^2}. \tag{23}$$

Alternatively, such an initial estimate can be obtained from the spread of a series of repeated measurements, as suggested in

Ref. [32]. However, as this does not quantify modelling uncertainties it is not suitable for the present study, and in particular for load case (B), where the one-dimensional approximation of the expansion chamber is known to have limitations [47,59].

In the present work, the aim is to obtain point estimates and uncertainty ranges for all unknowns. We use the maximum a posteriori estimate (MAP), which maximises the posterior probability density, the conditional mean (CM) of the unknowns, and the narrowest 95% credible intervals [53].

4. Results

This section presents the results of the parameter estimation for the melamine foam sample of interest, introduced in Section 2.2. The target experimental data consists of a single-observation dataset and a dual-observation dataset. The single-observation dataset consists of the sound absorption coefficient of the foam in load case (A), and the dual-observation dataset is composed of both the sound absorption coefficients corresponding to load cases (A) and (B), concatenated as specified in Eq. (12).

The following four paragraphs respectively present the incremental inversion results, a robustness study, the statistical inversion results and a comparison of multi-observation vs. single-observation estimations.

4.1. Incremental model inversion

The full frequency range of interest for load case (A) is here defined as $f \in [200, 4500]$ Hz. The low and high frequency limits are respectively chosen so as to avoid uncertainties in the inter-microphone phase and to limit the influence of the non-planar modes of the tube, whose first transversal resonance corresponds to the first azimuthal mode, i.e. (1,0) [47], at circa 5.7 kHz for the present setup. For load case (B), the main tube column imposes a non-zero transversal velocity along the central line of the expansion chamber and therefore azimuthal modes are not excited. The second transversal resonance of the expansion chamber occurs at the first radial mode, i.e. (0,1), at circa 2.65 kHz here, and therefore the upper frequency limit is chosen at 2 kHz.

Table 1 shows the frequency ranges obtained for the single observation and for the dual observation using the procedure described in Section 3.3.

Figs. 3 and 4 show the measured and estimated sound absorption coefficient for the single- and dual-observation cases, respectively, using a GCMMA implementation of the proposed incremental inversion approach with a random starting set of parameters. A good approximation of the measurement is achieved with the proposed model in both cases, with minor discrepancies at the low-frequency limit. These may be attributed to the model's inability to capture low-frequency dissipation effects in the impedance tube, or to the known limitations of the porous material model here used [17]. The figures depict as well the objective function as a function of the incremental inversion steps, and show generally increasing values due to the increasing sub-problem complexity.

The figures clearly show the effect of the elasticity of the frame on the sound absorption coefficient, observed for load case (A) as a dip at the elastic resonance of the material at 1351.56 Hz. The elastic effects also play an important role in load case (B), and arise as a peak at 1114.06 Hz. This is interpreted as a coupling effect between the expansion chamber and the material frame via the coupling tube. It is worth noting that a sufficient degree of sensitivity of load case (B) to the properties of the foam is crucial for the over-determination of the problem, as will be further explored in Section 4.4.

Table 1
Frequency intervals and tolerance criteria for the incremental inversion. (a) Single observation; (b) dual observation.

Step	$f_{\min}$ (Hz)	$f_{\max}$ (Hz)	$\delta_{f_{\text{obj}}}$	$\delta_{\mathbf{x}}$	n_{it}
		(a)			
1	200	669.53	10^{-2}	10^{-3}	2
2	200	1139.06	10^{-2}	10^{-3}	2
3	200	1351.56	10^{-2}	10^{-3}	2
4	200	3964.06	10^{-2}	10^{-3}	2
5	200	4500	10^{-2}	10^{-3}	2
6	200	4500	10^{-3}	10^{-4}	4
		(b)			
1	200	469.53	10^{-2}	10^{-3}	2
2	200	739.06	10^{-2}	10^{-3}	2
3	200	889.06	10^{-2}	10^{-3}	2
4	200	1114.06	10^{-2}	10^{-3}	2
5	200	1339.06	10^{-2}	10^{-3}	2
6	200	1526.56	10^{-2}	10^{-3}	2
7	200	1901.56	10^{-2}	10^{-3}	2
8	200	3964.06	10^{-2}	10^{-3}	2
9	200	4500	10^{-2}	10^{-3}	2
10	200	4500	10^{-3}	10^{-4}	4

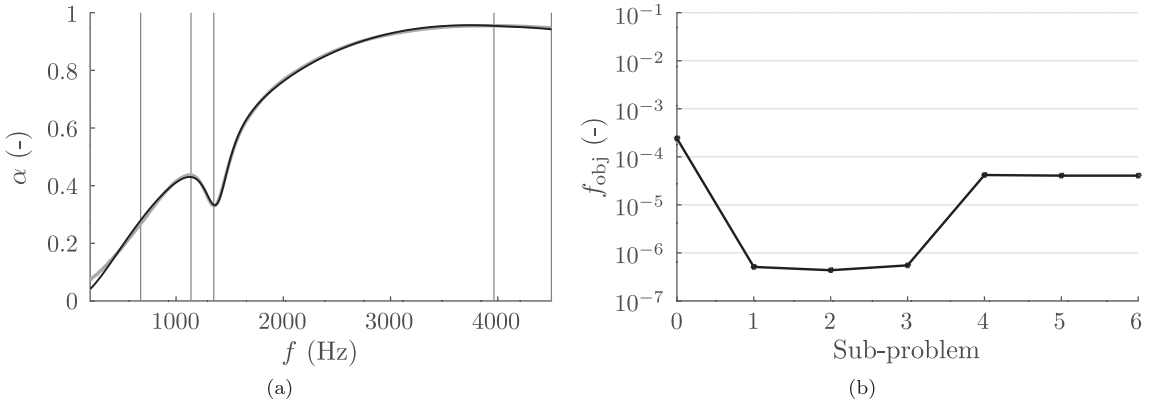

Fig. 3. Deterministic model inversion solution for a single-observation measurement of a rigid-backed poroelastic material in loading condition (A). (a) Sound absorption coefficient, ⋯⋯ measurement, —— model; (b) objective function history. The vertical lines represent the upper limits of the successive model inversion steps.

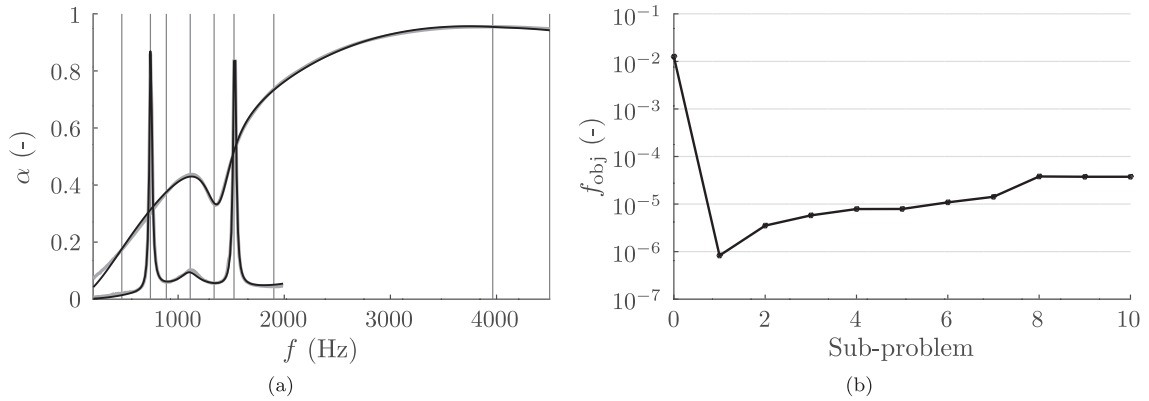

Fig. 4. Deterministic model inversion solution for the dual-observation measurement, including poroelastic material in loading condition (A) and poroelastic material coupled to expansion chamber in loading condition (B). (a) Sound absorption coefficient, ⋯⋯ measurement, —— model; (b) objective function history. The vertical lines represent the upper limits of the successive model inversion steps.

4.2. Robustness study

A multi-start approach [60] is here used in order to evaluate the robustness of the incremental search method, regardless of the initial guess of the parameter values. The procedure consists in repeating the model inversion process a number of times, here using a uniform random distribution for the parameter values as the starting point. Figs. 5 and 6 show the distribution of the parameter values obtained for 1000 runs of a full-range search versus the incremental search, for the single- and dual-observation cases respectively, and presented in the form of histograms. In addition, the distribution of objective function residuals and the solution time are also represented as histograms. An implementation based on SQP was preferred for this iterative procedure as the algorithm involves a lower computational overhead than the authors' implementation of GCMMA.

It can be observed that the incremental parameter search performs more consistently than the full-range search, especially in the dual-observation configuration. The appearance of multiple solutions elucidates the existence of local minima, which in turn results in a widening of the distribution of the objective function residuals. Nevertheless, the proposed incremental approach comes at a non-negligible computational cost. In the present case the expected solution time is approximately fivefold with respect to the full-range search.

4.3. Statistical model inversion

This paragraph presents the results of the Bayesian inversion approach, consisting in sampling the posterior density, see Section 3.4. For the present work, the target acceptance rate is set to $a_* = 0.2$. The Markov Chain Monte Carlo sampling algorithm is here initialised at the solution obtained from the incremental inversion. Although such a starting point is a feasible solution, a burn-in phase is considered in order to gather a sufficient number of samples for a reliable initial estimate of the covariance matrix of the unknowns. After the burn-in phase, the total number of samples kept for the analysis is set to $2 \cdot 10^6$. For the purposes of the problem of interest,

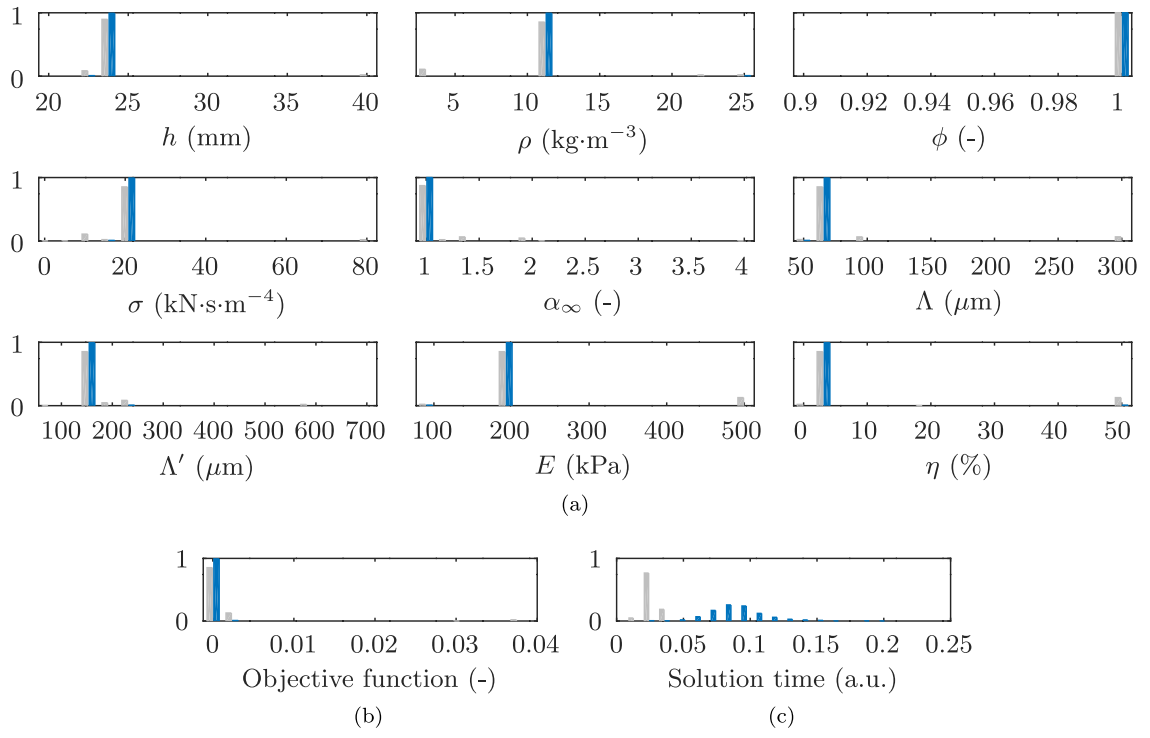

Fig. 5. Normalised histograms of parameter values, residual values and solution time for 1000 runs of the gradient-based single-observation case. Light grey, Full-range search; blue, incremental search.

two point estimates are extracted, namely the maximum a posteriori (MAP) and the conditional mean (CM). In addition, the 95% credible ranges of each model parameter are extracted.

Fig. 7 shows the pairwise 2D marginal densities for the 9 parameters of the poroelastic sample. The figure also includes the limits of the 95% credible ranges as well as the 1D marginal densities of the individual parameters. In addition, a measure of the inter-parameter correlation is provided thanks to the Pearson correlation coefficient, represented with the symbol P. It can be observed that the support of the densities is compact and presents a unique maximum point. Indeed, thanks to the incremental inversion solution being used as a feasible starting point, the mapping of other regions of the parameter space is avoided, and accordingly no multi-modal behaviour is observed.

A number of notable correlations among the parameters can be observed. For instance, the sample thickness exhibits a higher correlation with the acoustical transport properties than with the elastic properties. Indeed, the elasticity of the frame does not contribute to a global increase or decrease of the sound absorption coefficient, but locally via the frame resonance. Furthermore, the Young's modulus E and the mass density ρ are positively correlated, which is expected due to their joint control of the elastic resonance. The flow resistivity σ, the tortuosity α_∞ and the viscous characteristic length Λ are strongly correlated, as small variations in their values contribute to sound absorption in a comparable manner. In fact, a similar trend in the correlation of α_∞ and Λ has been reported [31]. In addition to these correlations, the thermal characteristic length Λ' and the Young's modulus E exhibit a strong correlation. Indeed, for the melamine foam here tested, the thermal and elastic effects are both dominant over a common mid-frequency range.

These correlations show the existence of a local interdependence of the model parameters. Several authors have reported on the scaling laws governing the constitutive properties of poroelastic media over small variations of the parameters [61–64]. For instance these scaling laws predict a positive correlation between the density and the mass density, between the flow resistivity and the tortuosity, and between the tortuosity and the viscous characteristic length, such as observed here. In addition to being intrinsic to the constitutive model, these parameter correlations may also be exacerbated by the choice of the sound absorption coefficient as the target data, as reported by Niskanen et al. [32].

The correlations observed here suggest that the model parameters are not independent of one another. As a matter of fact, a set of 3 independent parameters has been shown by Horoshenkov et al. [65] to be sufficient to correctly represent the acoustical behaviour of porous media, classically modelled using the 5-parameter JCA model herein [14,15], or the 6-parameter Johnson-Champoux-Allard-Lafarge (JCAL) model [14,15,17].

Fig. 8 shows the pairwise marginal densities for the dual-observation case. The additional parameters exhibit compact marginal densities and unique maxima as well, and introduce additional correlations. For instance, a high degree of correlation can be observed between l_b and η_b, which respectively account for low-frequency and broadband dissipation in the impedance tube. Similarly, r_e and η_e respectively account for absorption peak depth and broadband dissipation in the expansion chamber. Overall, a low correlation

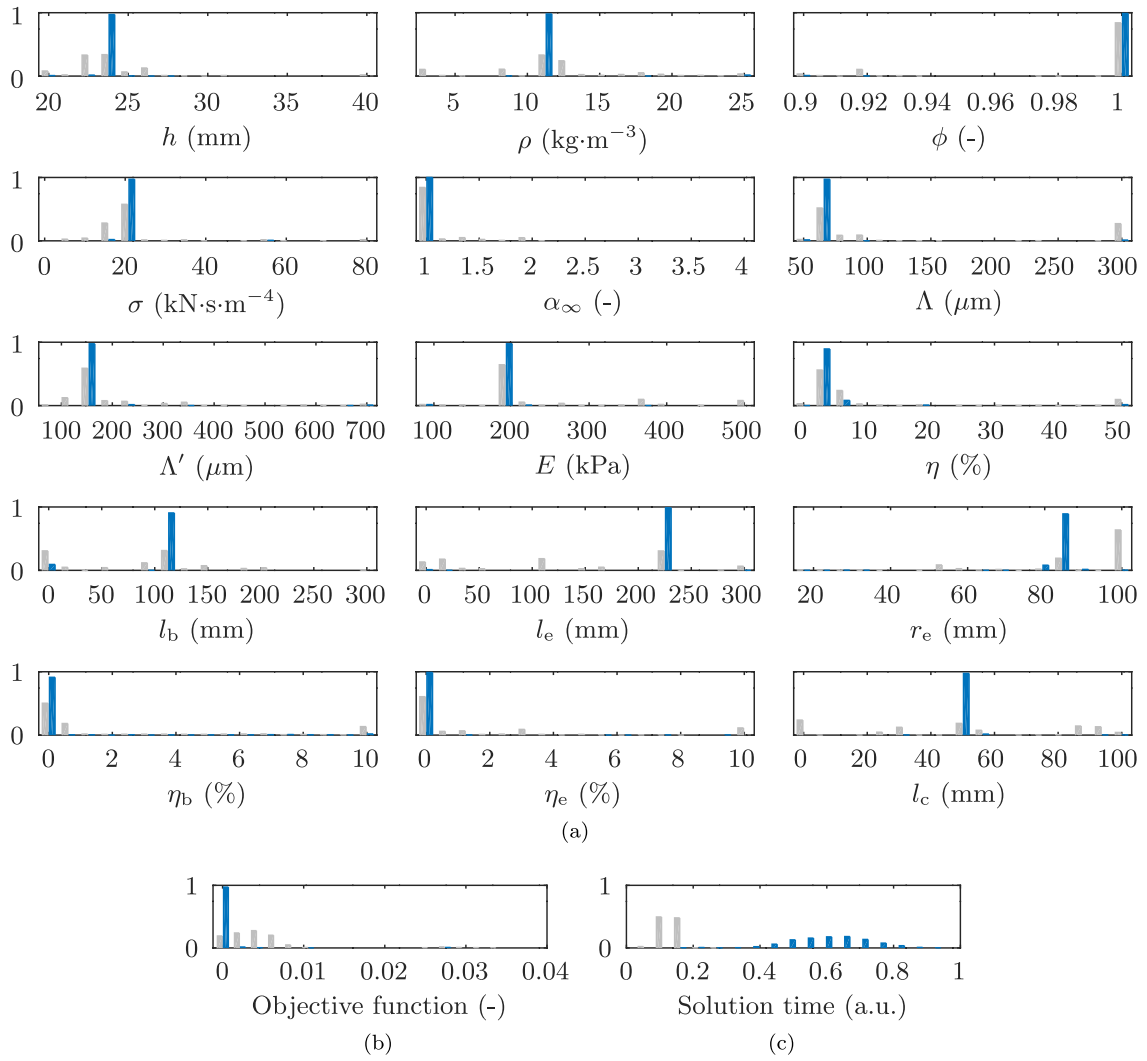

Fig. 6. Normalised histograms of parameter values, residual values and solution time for 1000 runs of the gradient-based multi-observation case. Light grey, Full-range search; blue, incremental search.

between the marginal densities of the poroelastic material parameters and those of the expansion chamber is observed. However, the coupling tube length l_c exhibits a somewhat higher correlation with E and ρ. This bears witness to the fact that the coupling tube strongly interacts with the elastic deformation of the foam.

4.4. Multi-observation vs. single-observation estimations

Table 2 displays the parameter values obtained for the deterministic incremental inversion as well as the MAP and CM estimates and the 95% credible intervals, for both the single- and dual-observation cases. In addition, Fig. 9 shows the marginal densities for all individual parameters, superimposed for the single- and dual-observation cases, as well as the credible intervals and MAP estimate values.

The obtained point estimates provide reasonable values for the different parameters of the poroelastic material model. Moreover, these are consistent with those reported elsewhere for melamine foams [5,25–27,32,39,66,67].

The most notable result of the present work is that the credible intervals obtained by the proposed method are narrower in the dual-observation case than in the single-observation case. This demonstrates that performing the measurement in two independent load cases effectively over-determines the inverse problem, in turn yielding an estimation with narrower parameter uncertainty ranges.

As a complement to the estimated model parameters, the ratio of characteristic lengths can be obtained from their sampled values. For the single observation, the MAP estimate is $\Lambda'/\Lambda = 2.241$ and the 95% credible interval is $\Lambda'/\Lambda \in [2.122, 2.326]$. The dual observation yields a MAP estimate of $\Lambda'/\Lambda = 2.246$, and a narrower 95% credible interval, $\Lambda'/\Lambda \in [2.162, 2.316]$. It is worth noting that the results with both observation approaches respect the well-established condition $\Lambda'/\Lambda \geqslant 2$ [40].

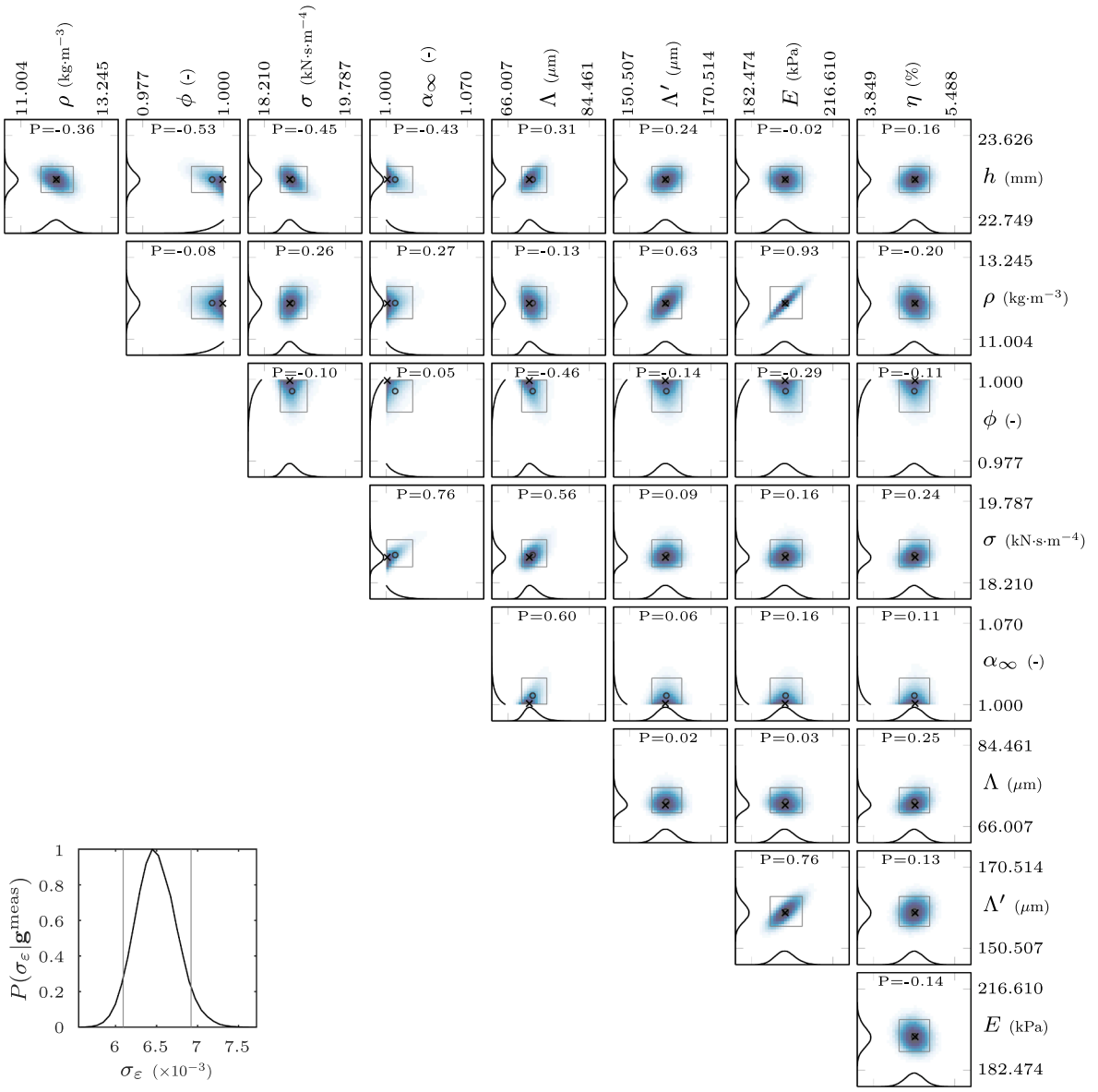

Fig. 7. Pairwise posterior marginal densities for the single-observation case. ——— Individual marginal densities; ------- credible ranges; × MAP estimate; ○ CM estimate; P, Pearson correlation coefficient. Bottom left: Posterior marginal density of the error ε.

In addition to the poroelastic material properties, the dimensions of the expansion chamber are obtained as a by-product of the method and can serve as part of the validation. In the present work we have chosen to introduce these geometrical properties as additional unknowns, but alternatively they could be assumed at their nominal values, albeit at the risk of introducing a bias in the values of the properties of the sample. Indeed, the present analysis shows that the geometrical parameters of the expansion chamber and coupling tube differ from their nominal values. For instance, the radius r_e of the expansion chamber presents an apparent over-estimation. In the opinion of the authors this arises as a compensation of one or both of the limitations of the model in this respect. The first possible cause is the well-known intrinsic inability of the classical transfer matrix method to correctly represent three-dimensional effects at sudden expansions [47,59], and the second is the unaccounted-for finite stiffness of the expansion chamber. It is worth noting that the uncertainty ranges in the manual measurements are directly derived using the precision of the length readings. This is naturally different from the statistical definition of 95% credible intervals, which prevents a rigorous comparison. Nevertheless, the measurements of lengths h, l_b, l_e and l_c overlap with the model inversion results. In particular, the length correction procedure correctly predicts the length of the coupling tube l_c and that of the primary tube section l_b.

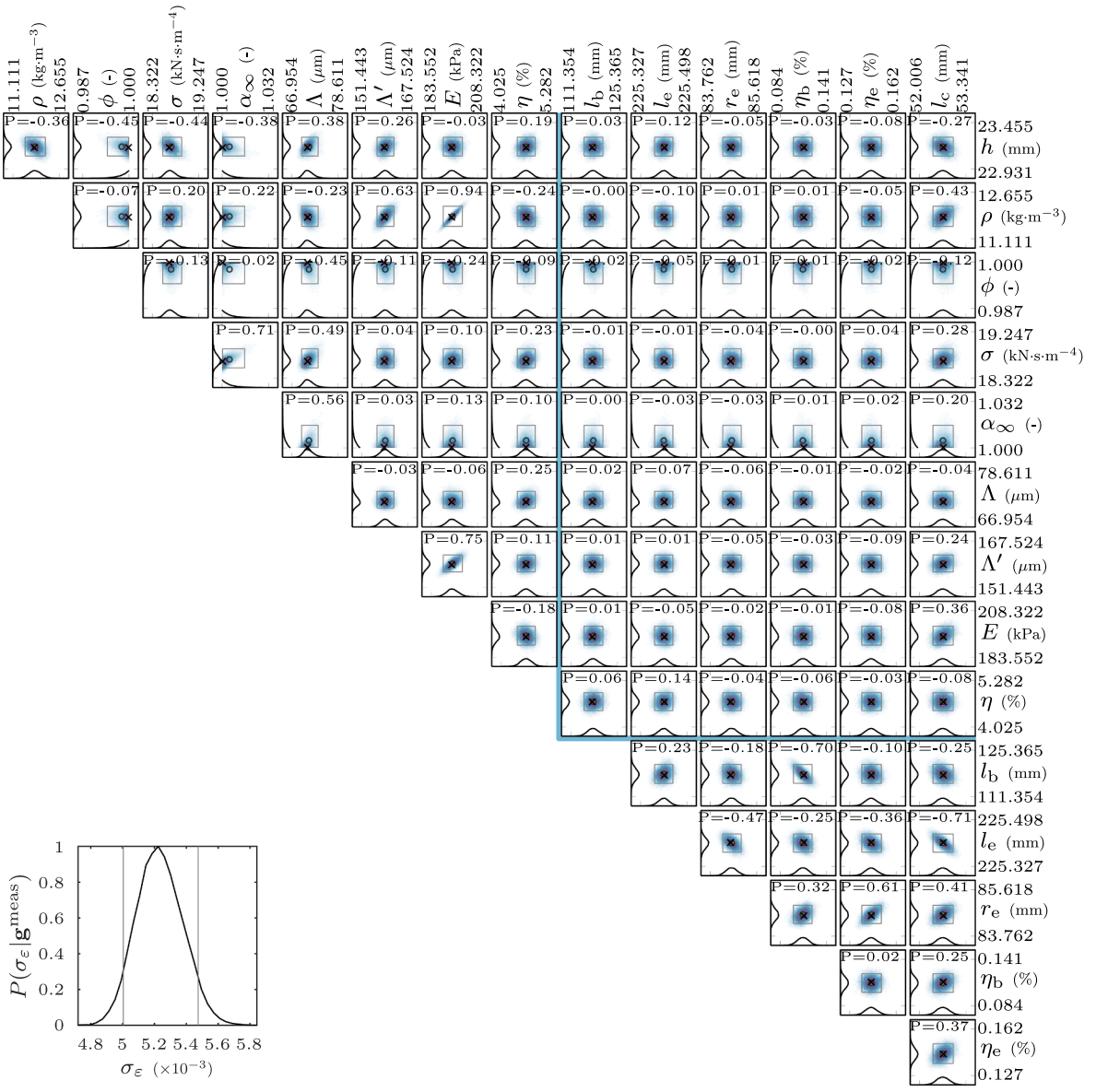

Fig. 8. Pairwise posterior marginal densities for the dual-observation case. —— Individual marginal densities; ·------· credible ranges; × MAP estimate; ○ CM estimate; P, Pearson correlation coefficient; ▬ delimitation of pairwise densities pertaining to the sample only, the load only, and the coupling of the two. Bottom left: Posterior marginal density of the error ε.

5. Summary of the findings

Based on the results above, the primary findings of this work can be summarised as follows. First, the proposed transfer matrix model of the system provides an accurate representation of the behaviour of the material sample under both loading conditions (A) and (B), thus enabling a good fit onto the experimental acquisitions while exhibiting sufficient sensitivity to all model parameters.

The proposed incremental inversion method has been shown to guarantee that the global solution of the problem is obtained independently from the initial guess, albeit at a significant computational cost as compared to a full-range search. This has been illustrated for both a single observation in load case (A) and a dual observation combining load cases (A) and (B).

Furthermore, the proposed framework for statistical model inversion provides marginal posterior densities for all unknowns of the problem. Accordingly, this enables a reliable extraction of point estimates and credible intervals. A notable demonstration of the robustness of the method is that the credible intervals for the single- and dual-observation cases overlap. More specifically, the point estimates for the single-observation case are systematically contained in the credible intervals of the dual-observation case, and vice versa.

The central result of this manuscript is the observation that the credible intervals are narrower in the case of the dual observation.

Table 2
Parameter values obtained from the deterministic incremental estimation and from the statistical inversion, including MAP estimate, CM estimate and 95% credible intervals. (a) Single observation; (b) dual observation.

Parameter	Unit	Determ.	MAP	CM	Cred. low	Cred. high
			(a)			
h	mm	23.14	23.14	23.15	23.01	23.29
ρ	kg·m^{-3}	11.865	11.958	11.994	11.562	12.449
ϕ	-	1.0000	0.9996	0.9966	0.9906	0.9998
σ	kN·s·m^{-4}	18.594	18.709	18.748	18.516	19.044
α_∞	-	0001	1.001	1.008	1	1.023
Λ	μm	69.53	70.93	71.61	69.09	74.82
Λ'	μm	158.66	159.07	159.46	155.92	163.24
E	kPa	194.199	196.697	196.715	190.276	203.756
η	%	4.618	4.696	4.671	4.364	4.982
σ_ε	10^{-3}	6.364	6.447	6.492	6.099	6.916
			(b)			
h	mm	23.17	23.18	23.18	23.08	23.29
ρ	kg·m^{-3}	11.766	11.821	11.846	11.512	12.190
ϕ	-	1.0000	0.9998	0.9980	0.9942	0.9999
σ	kN·s·m^{-4}	18.594	18.681	18.694	18.529	18.899
α_∞	-	0001	1.001	1.005	1	1.015
Λ	μm	69.91	70.65	71.22	69.38	73.47
Λ'	μm	159.07	159.75	159.62	156.75	162.62
E	kPa	193.228	194.352	194.792	189.792	200.025
η	%	4.662	4.716	4.702	4.456	4.950
l_b	mm	118.07	118.13	118.13	115.33	121.00
l_e	mm	225.41	225.42	225.41	225.38	225.45
r_e	mm	84.62	84.60	84.63	84.27	84.99
η_b	%	0.11	0.11	0.11	0.10	0.12
η_e	%	0.143	0.143	0.143	0.136	0.151
l_c	mm	52.61	52.68	52.68	52.38	52.98
σ_ε	10^{-3}	6.091	5.224	5.235	5.003	5.477

This shows that the use of a multi-observation dataset provides an over-determination of the inverse problem, thereby yielding refined uncertainty ranges on the unknowns.

A triple-observation model inversion was also performed, using an additional load case with a coupling tube of nominal length $\bar{l}_\mathrm{c} = 30$ mm. However, the results were comparable to the dual-observation case and no improvement was observed, presumably due to the fact that the additional load case did not significantly over-determine the inverse problem. These results are not reported here.

The application example shows that the method is capable of providing the full set of properties required to model macroscopically-homogeneous poroelastic media under the Biot-Johnson-Champoux-Allard model, with the exception of the Poisson ratio, from two-microphone impedance tube measurements. In the opinion of the authors, this achievement is of substantial value as previous methods rely on the assumption that one or more of these parameters are initially known, therefore removing the need for multiple test rigs.

Finally, in addition to point estimates and credible intervals, the statistical inversion framework allows for correlations among the parameters to be observed. Using the present results, these can be tied to a certain extent to the one-degree-of-freedom scaling laws for poroelastic media [61–64].

6. Conclusion

A multi-observation approach is here proposed, based on two consecutive measurements of the sound absorption coefficient of a rigid-backed sample of a poroelastic material, where in the second the sample is coupled to an expansion chamber. The methodology is shown to provide all 9 parameters of a comprehensive poroelastic material model, including the sample thickness and density, 5 transport parameters and 2 elastic properties. This is achieved through a combination of an incremental method designed to increase the complexity of a deterministic inverse problem gradually, and a statistical inversion framework providing the posterior probability density of the model parameters, from which point estimates, credible intervals and correlations are inferred. The results show reasonable credible intervals for all material parameters in accordance with values reported for melamine in the literature. Furthermore, the over-determination induced by the use of a multi-observation approach is shown to reduce the uncertainty in the parameter estimation. Additionally, the correlations observed among the porous material properties support the claim that the classical parametrisation of the acoustical behaviour of open-cell porous media is somewhat redundant and can be replaced with a model with fewer parameters [65].

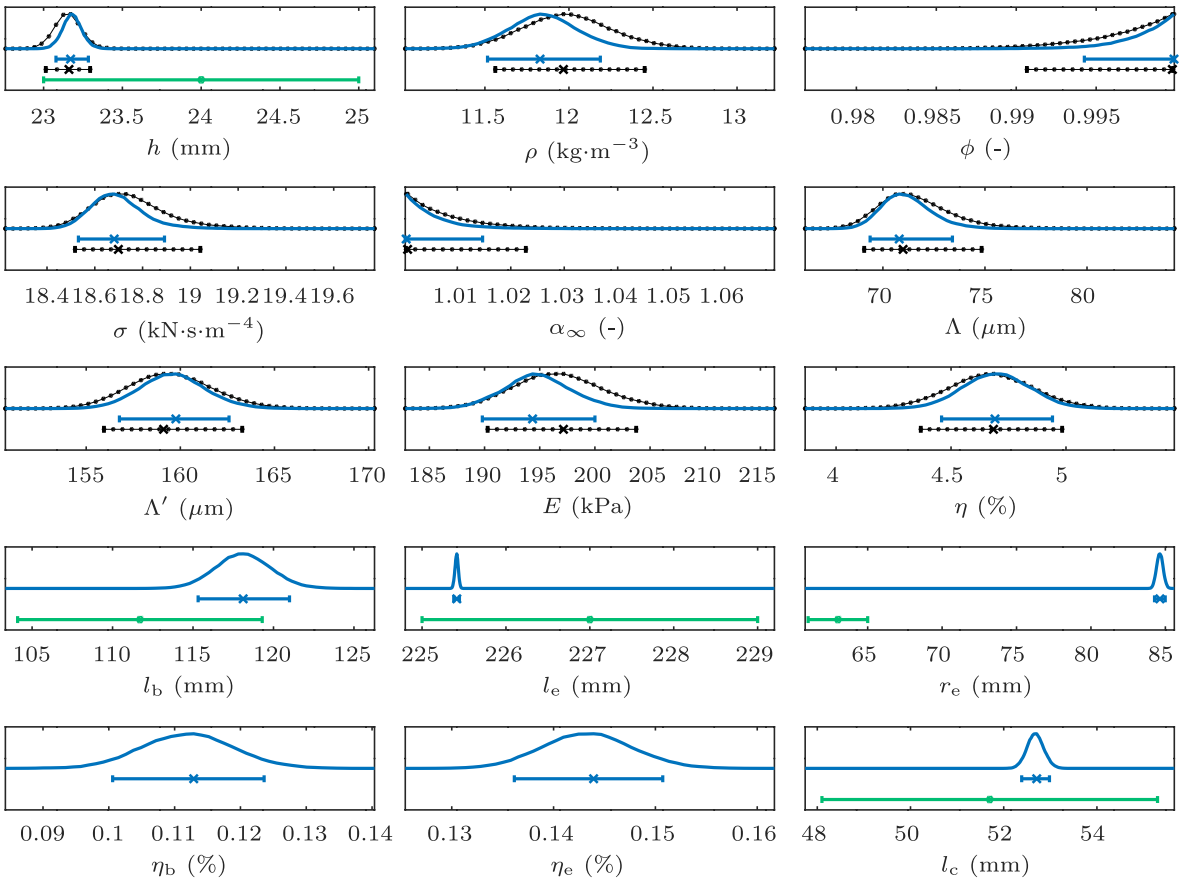

Fig. 9. Individual marginal densities for all model parameters. Single-observation, dual-observation. The horizontal error bars represent the credible ranges and the crosses denote the MAP estimate. Manual length measurement.

The method has been here illustrated for a melamine foam sample, for which the dimensions of the expansion chamber and coupling tube were suitable for enhancing fluid–structure interaction with the frame's elasticity. Applying the method to other materials may require different dimensions of the expansion chamber loading in order to promote a suitable degree of coupling. In future work, further over-determining the inverse problem could be achieved for instance by varying the expansion chamber length, which controls the major resonances of the coupled system.

In light of the results obtained by Niskanen et al. [32], the present method could be further applied to measurements in a three-microphone impedance tube with a rigid-backed sample, for instance using the processing proposed in Refs. [68,69]. This would enable the additional measurement of the equivalent density and bulk modulus, while ensuring a proper control of the boundary conditions.

It is worth noting that the proposed incremental inversion procedure is applicable to a wider variety of problems so long as modelling complexity can be treated gradually, for instance exploiting an asymptotic behaviour in high frequencies, or along other conditional variables of interest such as temperature or mechanical stress, for example.

Declaration of Competing Interest

The authors declare that they have no known competing financial interests or personal relationships that could have appeared to influence the work reported in this paper.

Acknowledgements

This article is based upon work initiated under the support from COST Action DENORMS CA-15125, funded by COST (European Cooperation in Science and Technology). The work has been supported by the Academy of Finland (Finnish Centre of Excellence of Inverse Modelling and Imaging and project number 321761) and by the Centre for ECO2 Vehicle Design at KTH, Vinnova Grant No. 2016–05195.

References

[1] ISO 10534-2. Acoustics – Determination of the sound absorption coefficient and impedance in impedance tubes – Part 2: Transfer-function method, 1998.
[2] ISO ISO 9053-1. Acoustics - Determination of airflow resistance - Part 1: Static airflow method, 2018.
[3] ISO ISO 9053-2. Acoustics - Determination of airflow resistance - Part 2: Alternating airflow method, 2020.
[4] C. Langlois, R. Panneton, N. Atalla, Polynomial relations for quasi-static mechanical characterization of isotropic poroelastic materials, J. Acoust. Soc. Am. 110 (6) (2001) 3032–3040.
[5] L. Jaouen, A. Renault, M. Deverge, Elastic and damping characterizations of acoustical porous materials: Available experimental methods and applications to a melamine foam, Appl. Acoust. 69 (12) (2008) 1129–1140.
[6] P. Leclaire, L. Kelders, W. Lauriks, M. Melon, N. Brown, B. Castagnède, Determination of the viscous and thermal characteristic lengths of plastic foams by ultrasonic measurements in helium and air, J. Appl. Phys. 80 (4) (1996) 2009–2012.
[7] P. Leclaire, L. Kelders, W. Lauriks, C. Glorieux, J. Thoen, Determination of the viscous characteristic length in air-filled porous materials by ultrasonic attenuation measurements, J. Acoust. Soc. Am. 99 (4) (1996) 1944–1948.
[8] P. Leclaire, O. Umnova, K. Horoshenkov, L. Maillet, Porosity measurement by comparison of air volumes, Rev. Sci. Instrum. 74 (3) (2003) 1366–1370.
[9] A. Moussatov, C. Ayrault, B. Castagnède, Porous material characterization–ultrasonic method for estimation of tortuosity and characteristic length using a barometric chamber, Ultrasonics 39 (3) (2001) 195–202.
[10] K.V. Horoshenkov, A review of acoustical methods for porous material characterisation, Int. J. Acoust. Vib. 22 (1) (2017) 92–103.
[11] R. Panneton, X. Olny, Acoustical determination of the parameters governing viscous dissipation in porous media, J. Acoust. Soc. Am. 119 (4) (2006) 2027–2040.
[12] X. Olny, R. Panneton, Acoustical determination of the parameters governing thermal dissipation in porous media, J. Acoust. Soc. Am. 123 (2) (2008) 814–824.
[13] P. Bonfiglio, F. Pompoli, Inversion problems for determining physical parameters of porous materials: Overview and comparison between different methods, Acta Acustica United Acustica 99 (3) (2013) 341–351.
[14] D.L. Johnson, J. Koplik, R. Dashen, Theory of dynamic permeability and tortuosity in fluid-saturated porous media, J. Fluid Mech. 176 (1987) 379–402.
[15] Y. Champoux, J.-F. Allard, Dynamic tortuosity and bulk modulus in air-saturated porous media, J. Appl. Phys. 70 (4) (1991) 1975–1979.
[16] L. Jaouen, E. Gourdon, P. Glé, Estimation of all six parameters of Johnson-Champoux-Allard-Lafarge model for acoustical porous materials from impedance tube measurements, J. Acoust. Soc. Am. 148 (4) (2020) 1998–2005.
[17] D. Lafarge, P. Lemarinier, J.F. Allard, V. Tarnow, Dynamic compressibility of air in porous structures at audible frequencies, J. Acoust. Soc. Am. 102 (4) (1997) 1995–2006.
[18] J.-P. Groby, E. Ogam, L. De Ryck, N. Sebaa, W. Lauriks, Analytical method for the ultrasonic characterization of homogeneous rigid porous materials from transmitted and reflected coefficients, J. Acoust. Soc. Am. 127 (2) (2010) 764–772.
[19] Y. Atalla, R. Panneton, Inverse acoustical characterization of open cell porous media using impedance tube measurements, Canad. Acoust. 33 (1) (2005) 11–24.
[20] T.G. Zieliński, Normalized inverse characterization of sound absorbing rigid porous media, J. Acoust. Soc. Am. 137 (6) (2015) 3232–3243.
[21] J.-P. Groby, O. Dazel, L. De Ryck, A. Khan, K. Horoshenkov, Acoustic characterization of graded porous materials under the rigid frame approximation. In Proceedings of Meetings on Acoustics ICA2013, volume 19, page 065009. Acoustical Society of America, 2013.
[22] M. Dossi, M. Brennan, M. Moesen, J. Vandenbroeck, L. Huo, An inverse method to determine acoustic parameters of polyurethane foams. In INTER-NOISE and NOISE-CON Congress and Conference Proceedings, volume 259, pages 1170–1181. Institute of Noise Control Engineering, 2019.
[23] K. Verdiere, R. Panneton, N. Atalla, S. Elkoun, Inverse poroelastic characterization of open-cell porous materials using an impedance tube. Technical report, SAE Technical Paper, 2017.
[24] J. Vanhuyse, E. Deckers, S. Jonckheere, B. Pluymers, W. Desmet, Global optimisation methods for poroelastic material characterisation using a clamped sample in a kundt tube setup, Mech. Syst. Signal Processing 68 (2016) 462–478.
[25] C. Van der Kelen, P. Göransson, Identification of the full anisotropic flow resistivity tensor for multiple glass wool and melamine foam samples, J. Acoust. Soc. Am. 134 (6) (2013) 4659–4669.
[26] C. Van der Kelen, J. Cuenca, P. Göransson, A method for the inverse estimation of the static elastic compressional moduli of anisotropic poroelastic foams - with application to a melamine foam, Polym. Testing 43 (43) (2015) 123–130.
[27] J. Cuenca, C. Van der Kelen, P. Göransson, A general methodology for inverse estimation of the elastic and anelastic properties of anisotropic open-cell porous materials — with application to a melamine foam, J. Appl. Phys. 115 (8) (2014), 084904.
[28] Z.E.A. Fellah, F.G. Mitri, M. Fellah, E. Ogam, C. Depollier, Ultrasonic characterization of porous absorbing materials: Inverse problem, J. Sound Vib. 302 (4–5) (2007) 746–759.
[29] L. De Ryck, W. Lauriks, P. Leclaire, J.-P. Groby, A. Wirgin, C. Depollier, Reconstruction of material properties profiles in one-dimensional macroscopically inhomogeneous rigid frame porous media in the frequency domain, J. Acoust. Soc. Am. 124 (3) (2008) 1591–1606.
[30] E. Ogam, Z. Fellah, N. Sebaa, J.-P. Groby, Non-ambiguous recovery of biot poroelastic parameters of cellular panels using ultrasonic waves, J. Sound Vib. 330 (6) (2011) 1074–1090.
[31] J.-D. Chazot, E. Zhang, J. Antoni, Acoustical and mechanical characterization of poroelastic materials using a Bayesian approach, J. Acoust. Soc. Am. 131 (6) (2012) 4584–4595.
[32] M. Niskanen, J.-P. Groby, A. Duclos, O. Dazel, J. Le Roux, N. Poulain, T. Huttunen, T. Lähivaara, Deterministic and statistical characterization of rigid frame porous materials from impedance tube measurements, J. Acoust. Soc. Am. 142 (4) (2017) 2407–2418.
[33] M. Niskanen, O. Dazel, J.-P. Groby, A. Duclos, T. Lähivaara, Characterising poroelastic materials in the ultrasonic range - A Bayesian approach, J. Sound Vib. 456 (2019) 30–48.
[34] R. Roncen, Z. Fellah, F. Simon, E. Piot, M. Fellah, E. Ogam, C. Depollier, Bayesian inference for the ultrasonic characterization of rigid porous materials using reflected waves by the first interface, J. Acoust. Soc. Am. 144 (1) (2018) 210–221.
[35] R. Roncen, Z.E.A. Fellah, D. Lafarge, E. Piot, F. Simon, E. Ogam, M. Fellah, C. Depollier, Acoustical modeling and bayesian inference for rigid porous media in the low-mid frequency regime, J. Acoust. Soc. Am. 144 (6) (2018) 3084–3101.
[36] R. Roncen, Z.E.A. Fellah, E. Piot, F. Simon, E. Ogam, M. Fellah, C. Depollier, Inverse identification of a higher order viscous parameter of rigid porous media in the high frequency domain, J. Acoust. Soc. Am. 145 (3) (2019) 1629–1639.
[37] C.J. Fackler, N. Xiang, K.V. Horoshenkov, Bayesian acoustic analysis of multilayer porous media, J. Acoust. Soc. Am. 144 (6) (2018) 3582–3592.
[38] K.V. Horoshenkov, A. Khan, F.-X. Bécot, L. Jaouen, F. Sgard, A. Renault, N. Amirouche, F. Pompoli, N. Prodi, P. Bonfiglio, et al., Reproducibility experiments on measuring acoustical properties of rigid-frame porous media (round-robin tests), J. Acoust. Soc. Am. 122 (1) (2007) 345–353.
[39] F. Pompoli, P. Bonfiglio, K.V. Horoshenkov, A. Khan, L. Jaouen, F.-X. Bécot, F. Sgard, F. Asdrubali, F. D'Alessandro, J. Hübelt, et al., How reproducible is the acoustical characterization of porous media? J. Acoust. Soc. Am. 141 (2) (2017) 945–955.
[40] J. Allard, N. Atalla, Propagation of Sound in Porous Media: Modelling Sound Absorbing Materials 2e, Wiley, 2009.
[41] P. Göransson, J. Cuenca, T. Lähivaara, Parameter estimation in modelling frequency response of coupled systems using a stepwise approach, Mech. Syst. Signal Process. 126 (2019) 161–175.
[42] J. Cuenca, P. Göransson, L. De Ryck, T. Lähivaara, Inverse parameter estimation in resonant, coupled fluid-structure interaction problems. In ISMA/USD, Leuven, 2018/9/17-19.
[43] J. Cuenca, L. De Ryck, P. Göransson, T. Lähivaara, Material parameter identification of coupled resonant systems using impedance tubes. In 26th International Congress on Sound and Vibration, Montreal, 7–11 July 2019.
[44] M. Brooks, Approximation complexity for piecewise monotone functions and real data, Comput. Math. Appl. 27 (8) (1994) 47–58.
[45] M. Bruneau, T. Scelo, Fundamentals of Acoustics, Wiley, 2013.
[46] O. Dazel, Numerical methods for the Biot theory in acoustics. Habilitation à diriger des recherches, Université du Maine, 2013.
[47] M. Munjal, Acoustics of Ducts and Mufflers With Application to Exhaust and Ventilation System Design, A Wiley-Interscience publication, Wiley, 1987.

[48] J. Rayleigh, The Theory of Sound. The Macmillan Company, 1896. Dover, New York, 1945.
[49] U. Ingard, On the theory and design of acoustic resonators, J. Acoust. Soc. Am. 25 (6) (1953) 1037–1061.
[50] L. Jaouen, F. Chevillotte, Length correction of 2D discontinuities or perforations at large wavelengths and for linear acoustics, Acta Acustica United Acustica 104 (2) (2018) 243–250.
[51] J. Nocedal, S. Wright, Numerical optimization, Springer Science & Business Media, 2006.
[52] K. Svanberg, A class of globally convergent optimization methods based on conservative convex separable approximations, SIAM J. Optim. 12 (2) (2002) 555–573.
[53] J. Kaipio, E. Somersalo, Statistical and Computational Inverse Problems, Springer-Verlag, 2005.
[54] D. Calvetti, E. Somersalo, Introduction to Bayesian Scientific Computing: Ten Lectures on Subjective Computing (Surveys and Tutorials in the Applied Mathematical Sciences), Springer-Verlag, 2007.
[55] H. Haario, E. Saksman, J. Tamminen, Adaptive proposal distribution for random walk Metropolis algorithm, Comput. Stat. 14 (1999) 375–396.
[56] H. Haario, E. Saksman, J. Tamminen, An adaptive Metropolis algorithm, Bernoulli 7 (2001) 223–242.
[57] A. Gelman, G.O. Roberts, W.R. Gilks, Efficient metropolis jumping rules. Bayesian, Statistics 5 (599–608) (1996) 42.
[58] C. Andrieu, J. Thoms, A tutorial on adaptive MCMC, Stat. Comput. 18 (4) (2008) 343–373.
[59] M. Alkmim, J. Cuenca, L. De Ryck, P. Göransson, Model-based acoustic characterisation of duct components and extrapolation to inhomogeneous thermal conditions, In ISMA/USD, 2018/9/17-19.
[60] F.W. Glover, G.A. Kochenberger, editors. Handbook of metaheuristics, volume 57. Springer Science & Business Media, 2006.
[61] L.J. Gibson, M.F. Ashby, Cellular solids: structure and properties, Cambridge University Press, 1999.
[62] P. Göransson, Acoustic and vibrational damping in porous solids, Phil. Trans. R. Soc. A: Math., Physical Eng. Sci. 364 (1838) (2006) 89–108.
[63] E. Lind-Nordgren, P. Göransson, Optimising open porous foam for acoustical and vibrational performance, J. Sound Vib. 329 (7) (2010) 753–767.
[64] C.J. Cameron, E.L. Nordgren, P. Wennhage, P. Göransson, On the balancing of structural and acoustic performance of a sandwich panel based on topology, property, and size optimization, J. Sound Vib. 333 (13) (2014) 2677–2698.
[65] K.V. Horoshenkov, A. Hurrell, J.-P. Groby, A three-parameter analytical model for the acoustical properties of porous media, J. Acoust. Soc. Am. 145 (4) (2019) 2512–2517.
[66] N. Geebelen, L. Boeckx, G. Vermeir, W. Lauriks, J.F. Allard, O. Dazel, Measurement of the rigidity coefficients of a melamine foam, Acta Acustica United Acustica 93 (5) (2007) 783–788.
[67] L. Boeckx, P. Leclaire, P. Khurana, C. Glorieux, W. Lauriks, J.-F. Allard, Investigation of the phase velocities of guided acoustic waves in soft porous layers, J. Acoust. Soc. Am. 117 (2) (2005) 545–554.
[68] T. Iwase, Y. Izumi, R. Kawabata, A new measuring method for sound propagation constant by using sound tube without any air spaces back of a test material, In INTER-NOISE and NOISE-CON Congress and Conference Proceedings, volume 1998, pages 1265–1268. Institute of Noise Control Engineering, 1998.
[69] Y. Salissou, R. Panneton, O. Doutres, Complement to standard method for measuring normal incidence sound transmission loss with three microphones, J. Acoust. Soc. Am. 131 (3) (2012) EL216–EL222.